Korean J. Chem. Eng., **29**(10), 1321-1328 (2012)
DOI: 10.1007/s11814-012-0025-0

Convective heat transfer of alumina nanofluids in laminar flows through a pipe at the thermal entrance regime

Seokwon Kim, Hansol Yoo, and Chongyoup Kim†

Department of Chemical and Biological Engineering, Korea University, Anam-dong, Sungbuk-gu, Seoul 136-713, Korea
(*Received 10 January 2012 • accepted 29 February 2012*)

Abstract–The convective heat transfer characteristics of aqueous alumina nanofluids were investigated experimentally under forced laminar tube flows. The particles had different shapes of cylinders, bricks and blades, and particle loading was between 0-5 volume%. The nanofluids were characterized rheologically, and the heat transfer system was validated by using water without particles. In calculating Nusselt and Peclet numbers to assess heat transfer enhancement of nanofluids, physical properties of water were used so as not to exaggerate the amount of heat transfer. It was found that heat transfer coefficients of nanofluids are almost the same or a little smaller than that of water. The heat transfer coefficient can be reduced by the lowering the thermal conductivity of the nanofluid under shearing conditions and particle depletion by the cluster migration from the wall to the tube center. The reduction in thermophysical properties also contributes to the reduction in heat transfer coefficient. It has been concluded that nanofluids from metal particles with appropriate stabilizing agents can satisfy the requirements to be a practically usable nanofluid.

Key words: Leveque Problem, Dispersion, Gel, Migration, Thermal Conductivity

INTRODUCTION

A nanofluid is a kind of colloid consisting of nanometer-sized particles dispersed in a traditional heat transfer fluid such as water, ethylene glycol, or mineral oil. Nanofluids may be useful as heat transfer fluids due to their higher thermal conductivities compared with pure liquid [1]. In practical applications of nanofluids, convective heat transfer and friction loss are important factors. The forced convection problem in a laminar tube flow of a Newtonian fluid with a constant heat flux is well documented and the Nusselt numbers for the entrance and fully developed regimes are given as follows [2]:

$$\text{Entrance regime: } Nu = 1.640\left(\frac{R}{z}\right)^{1/3} Pe^{1/3} \quad (1)$$

$$\text{Fully developed regime: } Nu = 4.364 \quad (2)$$

Another important issue is the friction loss. In a laminar flow of Newtonian fluid, the fanning friction factor $f=(|\Delta p|/2\rho v^2)(D/L)$ and Reynolds number $Re=Dv\rho/\mu$ have the following relationship:

$$f = \frac{16}{Re} \quad (3)$$

Here, D and L are the inner diameter and length of tube, v is velocity, ρ is fluid density, and μ is the viscosity of the fluid. The relations (1) and (3) will be used as references in assessing the characteristics of nanofluids. In the case of nanofluids, the definition of a dimensionless group such as Nu, Re, Pr or Pe can be ambiguous since the material properties are flow dependent. These issues can cause large discrepancies in the heat transfer coefficient (h) among reports. The convective heat transfer is influenced by the increase in viscosity and non-Newtonian behavior that occurs when particles are added to a fluid. Some nanofluids show high thermal conductivities and Newtonian behavior with low viscosities [3-9], while some other nanofluids show non-Newtonian behavior [3,8,10-13]. Also, there have been controversies over the magnitude of the increase in convective heat transfer coefficient. In some cases it was almost the same as, or even a little smaller than that of a pure liquid. It appears that the convective heat transfer coefficient can change sensitively with dispersion status. In the following we will separately review two cases which are contrary to each other.

Xuan and Li [14] reported that a water base nanofluid with 100 nm copper nanoparticles showed 60% increase in h when the volume fraction (ϕ) of nanoparticles was 0.02. In this case they used k and η of nanofluids in calculating Nu and Re. However, it should be noted that, if the viscosity of water is used in calculating Re, there should be 30% decrease in h. Wen and Ding [15] reported that there was 25-38% increase in h at the entrance regime when 1.6 volume% of 43 nm copper particles were dispersed in aqueous solution of sodium dodecyl sulfate and the Re was between 710 and 1940. However, this report contained as large as 40% error at low Re and 10% at Re>2,000, even in the case of pure water compared with the well established theory by Shah [16]. Ding et al. [11] reported that a nanofluid of 0.5 wt% multi-walled carbon nanotube (MWCNT) dispersed in an aqueous solution of gum arabic 350% increase was observed when Re=800. It was suggested that the large enhancement could be due to the high aspect ratio of the CNTs, rearrangement of particles, shear induced thermal conduction enhancement, and a reduction of the thermal boundary induced by the nanoparticles. In the case of nanofluids of alumina nanoparticles, 40% increase was observed when ϕ=0.03 [17]. In this case the increase in k from

†To whom correspondence should be addressed.
E-mail: cykim@grtrkr.korea.ac.kr

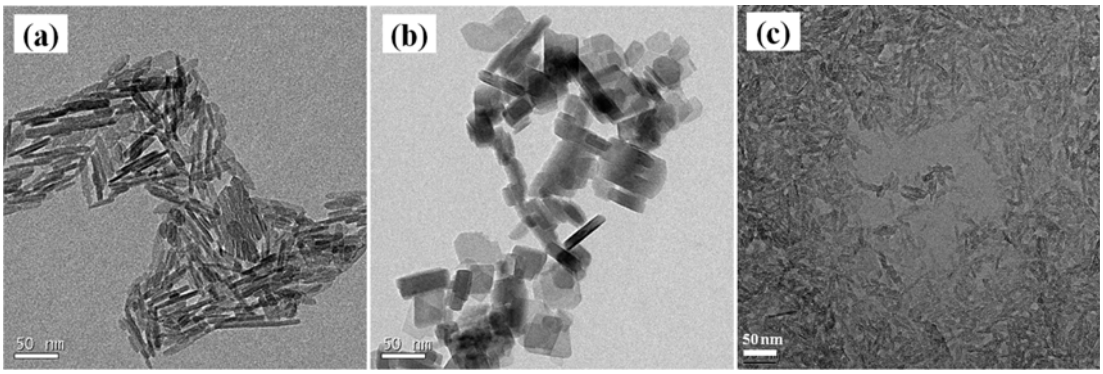

Fig. 1. TEM images of alumina nanoparticles: (a) cylinder, (b) brick, (c) blade.

the pure fluid was 15%. This means that even a larger increase can be expected than the increase in k itself. In addition to aforementioned reports there have been more reports on the enhancement of h from the value of the pure fluid [18-24].

The convective heat transfer of MWCNT nanofluids in SDS aqueous solution was studied by Faulkner et al. [25] with a micro channel of 335 μm in diameter. When 2<Re<17, h varied from half to twice of h of pure water. Graphite (aspect ratio~0.02) nanofluids showed similar tendencies: A 2.5 wt% graphite nanofluid showed 20% higher h than that of the commercial automatic transmission fluid which was used as the base fluid. However, in the case of a 2.0 wt% nanofluid in another base fluid, h was 10% less than that of the base fluid. Yang et al. [26] suggested that the solvent dependency could be related to the percolation limit of the particle concentration. Rea et al. [27] reported that an alumina nanofluid (ϕ= 0.06) showed 27% higher convective heat transfer than pure liquid. However, at all particle concentrations of zirconia nanofluids, h's were 5% less than that of pure liquid. Rea et al. also argued that it was because the product of density and heat capacity became smaller while the thermal conductivity increased little with increasing particle concentration. Ferrouillat et al. [28] suggested that the heat conduction in the axial direction could be another reason for the reduced h.

As described above, there have been controversies over the enhancement of h of nanofluid. Such controversies are believed to be due to insufficient characterization of nanofluids as well as inappropriate definition of relevant dimensionless numbers. In the usage of nanofluids what is important is whether more heat is transferred or not while using the same amount of nanofluid instead of a conventional heat transfer fluid. The increase in Nusselt number does not have any meaning without net increases in transferred heat. Noting these two important points, in the present study, laminar forced convection of nanofluids from three different shapes of alumina particles, cylinder, brick, and blade, dispersed in de-ionized water is investigated experimentally at the thermal entrance regime. Re was in the range of 200 and 1600. The dispersion status of the nanofluids was characterized by rheological measurements, TEM and dynamic light scattering (DLS) techniques. The result shows that the net amount of heat transfer could decrease by adding nanoparticles to conventional heat transfer fluids, and the decrease was caused by the changes in thermophysical properties and/or change in microstructure during the flow through a pipe.

EXPERIMENT

1. Materials

Nanofluids were prepared by dispersing alumina nanoparticles in deionized water. The nanoparticles were donated from Sasol North American Inc. The nanoparticles had different shapes. The aspect ratios of cylinder, brick, and blade particles were approximately 5, 1, and 6, respectively, and can be confirmed from TEM images shown in Fig. 1. The volume fraction (ϕ) was 0.01, 0.03 or 0.05. A proper amount of nanoparticles was dispersed in 1,500 ml water in a 2,000 ml beaker while stirring for 24 hrs by an 8 cm magnetic bar over a stirring plate (Corning, Laboratory stirrer/hot plate PC620) following the manufacturer's suggestion. Then the sample was sonicated (Sonics and Materials Inc., VCX-750, 750 W, 60% amplitude, T< 40 °C) for 30 mins and left under gravity for 1 hr before measurements were taken. When the nanofluid is prepared by this method it has been known that primary particles and aggregates coexist in the nanofluid by transmission electron microscopy (TEM) and dynamic light scattering (DLS) [29]. The density and heat capacity of the nanofluid were obtained by assuming the linear mixing rule in particle volume fraction as follows:

$$\rho_{NF}=\phi\rho_p+(1-\phi)\rho_{water} \tag{4}$$

$$C_{p,NF}=\frac{\phi\rho_p C_{p,p}+(1-\phi)\rho_{water}C_{p,water}}{\rho_{NF}} \tag{5}$$

2. Equipment

A recycling system was designed so that the required amount of nanofluid was minimal as shown in Fig. 2. The system consists of a reservoir, a tube wrapped with an electric heater of 1 kW, a pump, a cooling coil and a data acquisition system (Agilent Tech., 34970A) together with connecting tubes and sensors. As the heated tube a stainless steel tube (SUS316) of 3/8 inch in outer-diameter (The inner diameter is 7.0 mm) and 2.0 m in length was used. The pressure drop was measured by a differential pressure transducer (Siemens, SITRANS PDS-III series, 2.5-250 mbar) between two positions of 0.75 m apart. The flow rate was measured by a catch-and-weigh method. A gear pump (Micropump Corp., GB-P35JVSA head) was used to control flow rate and minimize fluctuation. The temperature of the fluid was measured by T-type thermocouples. The liquid temperature was measured at the outlet of the reservoir, before and after the pressure difference measurement.

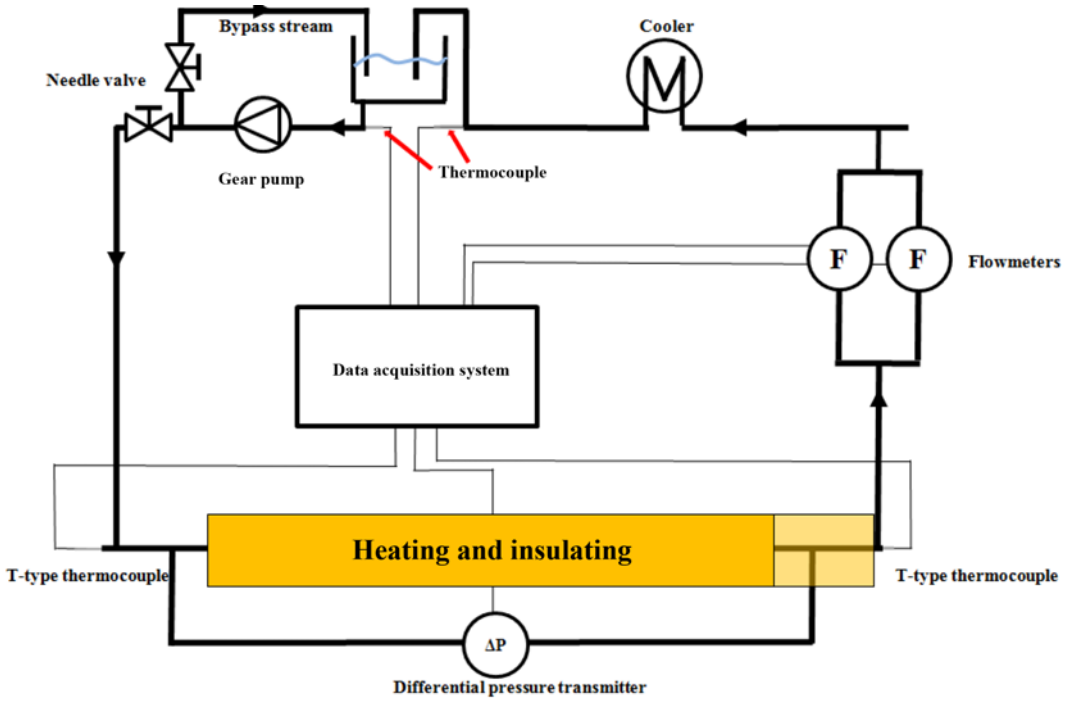

Fig. 2. Heat transfer coefficient measurement system.

3. Convective Heat Transfer Coefficient Measurement

There were 11 positions (0.005 m, 0.057 m, 0.156 m, 0.257 m, 0.445 m, 0.700 m, 0.944 m, 1.232 m, 1.485 m, 1.733 m, and 2.000 m) at which the wall temperatures were measured along the axial direction of the tube. To measure the wall temperature precisely, thermocouples were placed at a narrow well drilled to 500 μm of the tube inner wall. Thermocouple wells were first covered with epoxy electrical insulation. Thermocouple junctions were inserted and then covered with a thermo-conductive silver paste. We did not use the conventional Joule heating method in which an electric potential should be applied between tube ends to generate heat along the metal tube to supply a constant heat flux. It can cause a large error since the electric potential is also applied to the nanofluids which are basically electrolytes, and hence heat can be generated inside the nanofluids. To apply a constant heat flux to the tube wall, an electric serial heater of 10 m in length and 0.002 m in thickness was coiled around the tube. Ceramic wool of 0.025 m and a polyethylene insulator of 0.003 m thickness were wrapped around the tube. Finally, the insulated tube was covered with an insulating tape to minimize heat loss from the heater. When there is no heat loss the fluid temperatures (T_{in} and T_{out}), flow rate Q and the electric heat input q have the following relation:

$$\rho C_p Q(T_{out} - T_{in}) = V \times I = q \quad (6)$$

When we measured the outlet temperature from the tube, the fluid was mixed using a vortex generator placed in the tube. In other words, we measured the mixing-cup temperature. The environment temperature and the fluid temperature were kept at 25 °C using an air conditioner and a water bath, respectively. Under these conditions, we found about 10% of heat loss compared with the applied electricity from the AC power supply. The heated fluid was cooled by passing through a cooling coil (a stainless steel corrugated tube of 3 m in length and 0.015 m in outer-diameter) immersed in a cooling bath. The flow became steady after a minute of pumping.

RESULTS AND DISCUSSION

We first measured the rheological properties of nanofluids by using a rotational rheometer. In Fig. 3 the viscosities of nanofluids show severe shear-thinning or Newtonian behavior, depending upon particle shape or particle loading. The viscosity of the dispersion of cylindrical particles at ϕ=0.01 is almost the same as that of dispersions of other shapes of particles at ϕ=0.05 and is also Newtonian. Ten (10) - 40% higher viscosity is observed for the blade dispersion than the viscosity of the brick dispersion. This may be partly due to the high aspect ratio of the blade. Since some particles exist

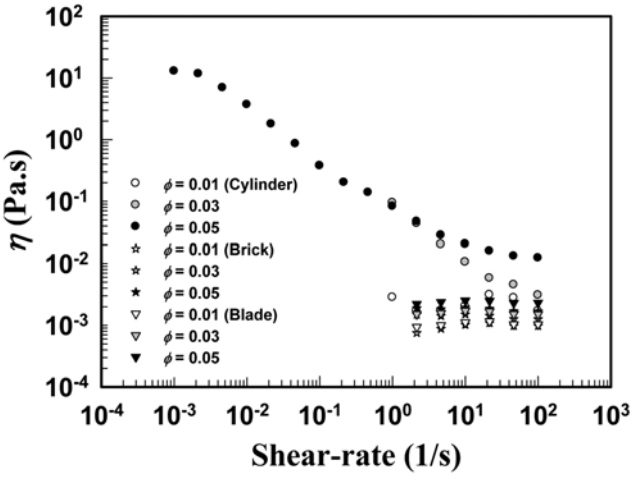

Fig. 3. Shear-viscosities of three different Al_2O_3 nanofluids.

as aggregated forms, the expected large difference appears to be shaded. The viscosity of the cylindrical particle dispersion at ϕ= 0.05 shows strong shear thinning behavior. The zero shear viscosity is about four orders larger than the water viscosity while the infinite shear viscosity is about 10 times larger. This means that the nanofluid becomes a weak gel [29].

In Fig. 4, the friction factors of the nanofluids are plotted in the laminar regime. In calculating Reynolds numbers for nanofluids we used the viscosity of water without particles. If the viscosity of nanofluid is used, Re becomes smaller due to the high viscosity of nanofluid, and then the friction factor of nanofluid at the smaller Re could be the same as or even smaller than that of water at this low Re. Then it can appear that the pressure drop of nanofluid flow is not larger than that of water even though the real pressure drop is higher. This should be nonsense. Therefore, the water viscosity was used in calculating Re not to induce any confusion in assessing nanofluids by the pressure drop change. A similar method has been used in assessing the drag reduction of polymer. In this case due to dissolved polymer the viscosity increases and becomes shear thinning to show the same situation as in the case of suspension [30]. In the laminar regime the friction factor increases slightly with particle concentration as expected, while the slope is similar to the line for water. One may expect that |df/d Re| of the nanofluid should be larger than that of pure water due to the shear-thinning property of nanofluids. It appears that a microstructure develops inside the tube and hence the velocity profile is affected by the microstructure. The microstructure can be developed by particle migration in a nonhomogeneous flow field. Since many of the nanoparticles exist as aggregates and the Brownian diffusion should be not large for the aggregate, particles can migrate toward the center of tube, overcoming the Brownian back diffusion. Therefore, the viscosity of nanofluid near the wall becomes lower. This will shade the strong shear thinning property of nanofluid.

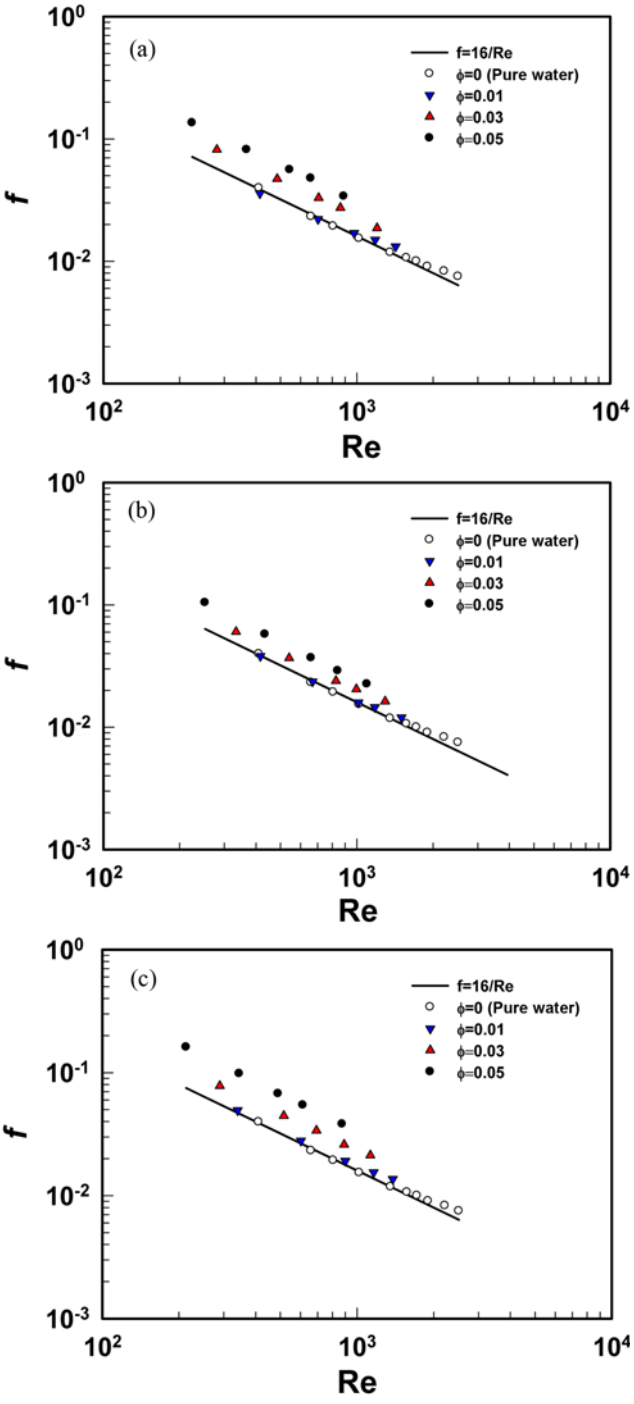

Fig. 4. Friction factor with Re in tube flow of nanofluids of different shapes: (a) cylinder, (b) brick, (c) blade.

The experiments were performed within the thermal entrance regime. It is known that it belongs to the thermal entrance regime when Graetz number defined below is much larger than 1 [2]:

$$Gz = \frac{\pi}{4}RePr\frac{D}{L} = \frac{\pi D}{4L}Pe \tag{7}$$

The present experiments were performed for 2<Gz<30, and hence most of the experiments are considered to be in the entrance regime. The effect of viscous dissipation was also examined. In the case of the 5% cylinder dispersion for which the viscosity is the highest among the samples, the effect was found to be negligible since the Brinkman number [31], $Br=V_{avg}^2\mu/q''_{ref}D_h$ was as low as 2.7×10^{-3}. Here q″ is the heat transferred per unit time and unit area.

Before performing experiments with nanofluids, we first carried out the validation of the system with water. While supplying a constant heat flux of 600-700 W/m^2 to the tube, we measured the temperature distribution along the tube. From the measured temperature profile at the steady state and the fully developed conditions we calculated the local heat transfer coefficient h_{local} as a function of axial position as well as the average heat transfer coefficient h defined as follows:

$$h_{local} = \frac{\rho C_p Q(T_{out} - T_{in})}{\pi DL(T_W - T_{avg})} \tag{8}$$

$$h = \frac{\rho C_p Q(T_{out} - T_{in})}{\pi DL(T_W - T_{avg})_{LM}} \tag{9}$$

In determining the local heat transfer coefficient it is assumed that the average temperature of the fluid increases linearly with distance in the axial direction by assuming that heat loss to the environment is uniform as shown in Eq. (10):

$$T_{avg} = T_{in} + \frac{(T_{out} - T_{in})z}{L} \tag{10}$$

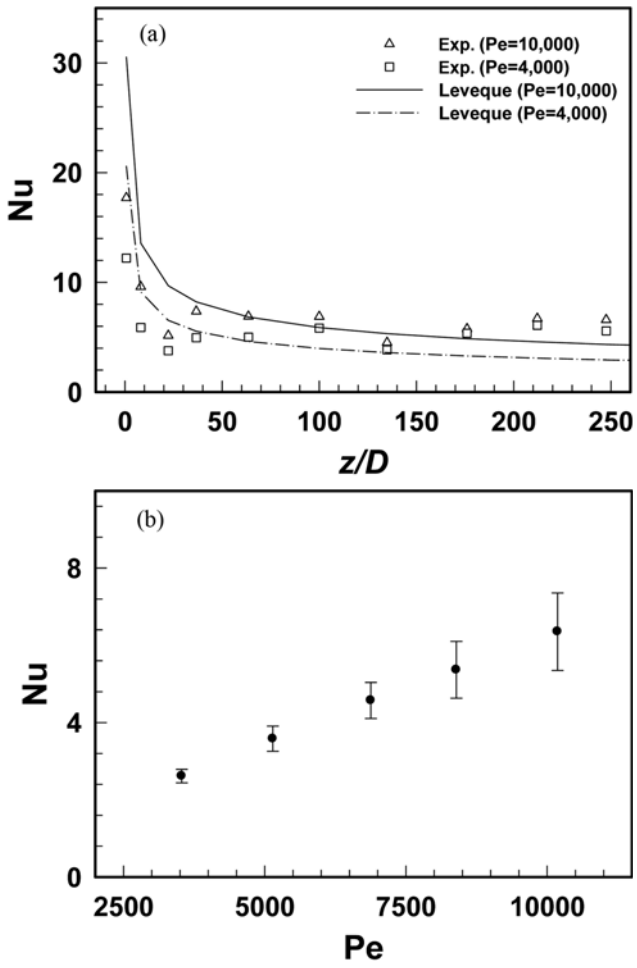

Fig. 5. Convective heat transfer characteristics for the laminar flow of water. (a) Local Nu vs. z/D at two different values of Pe, (b) Average Nu variation with Pe.

This should be a reasonable assumption since the ribbon heater was wrapped uniformly around the tube.

Fig. 5(a) shows the local Nusselt number of water. In the Figure, z is position in the axial direction and D is the inner-diameter of the tube. The local Nusselt number is larger for higher Pe as expected. The measured Nu_{local} values are reasonably matched to the Leveque approximation [2] in the range 40<z/D<130. When z/D is smaller than 40 the measured values are smaller than the Leveque's solutions, while the measured values are larger than the Leveque's solutions when z/D is larger than about 150. The deviations appear to be caused by the diffusion of heat along the axial direction through the wall and fluid. At the entrance region a large amount of heat can be conducted to the upstream side of the tube by conduction through the metallic wall, and this heat is conducted radially to the fluid. Therefore, the wall temperature at the inlet will become lower than the value without the conduction. There is also heat conduction to the upstream fluid, even though it is assumed that the inlet temperature is the same as the value at the far upstream. Therefore, the heat flux, in other words Nu_{local}, at the inlet region reads smaller than the theoretical prediction. The converse is true at the exit region, and hence Nu_{local} is larger than the theoretical prediction. Fig. 5(b) shows the average Nusselt number. These values will be compared with convective heat transfer characteristics in nanofluids.

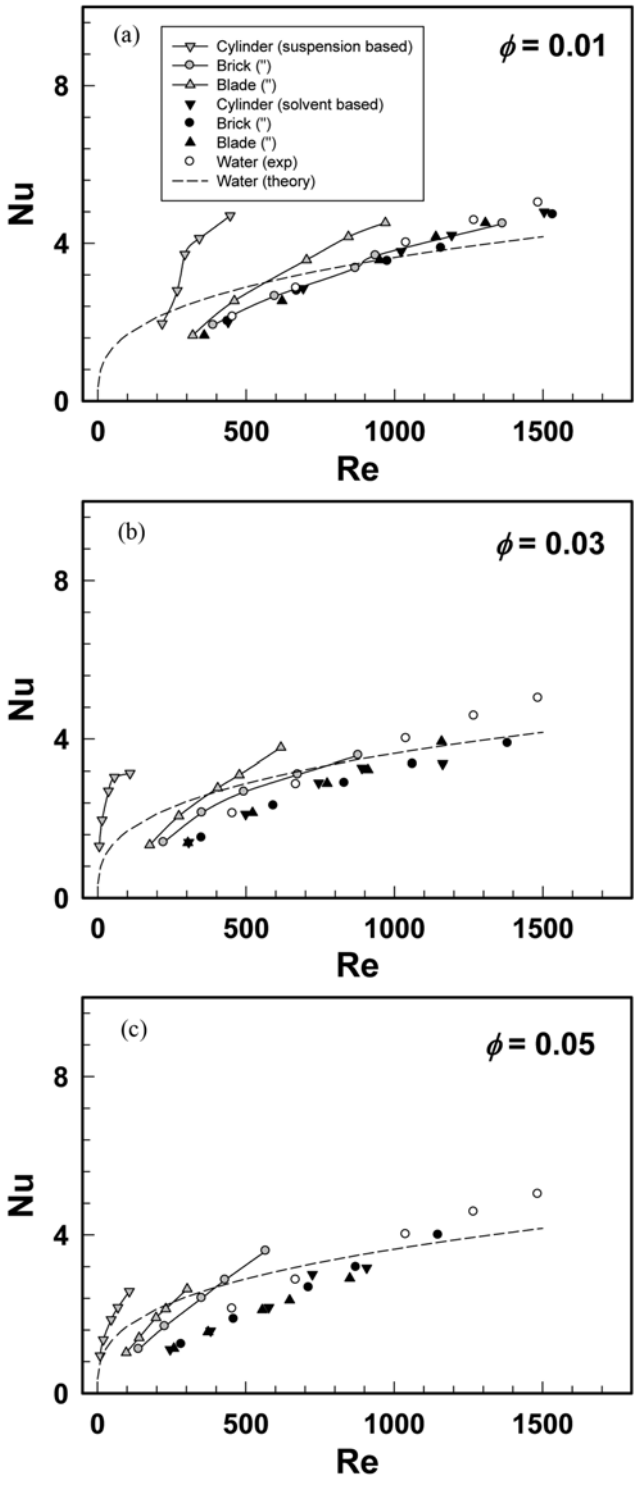

Fig. 6. Effects of primary particle shape on the heat transfer characteristics of nanofluids at different particle loading. (a) 1%, (b) 3%, (c) 5%.

Fig. 6 shows the change in Nusselt number with Reynolds number for nanofluids of various nanoparticle shapes and particle loading. Here Nu and Re were calculated based on the properties of nanofluids (Grey symbols) temporarily. Specifically, zero shear or shear rate independent viscosity was used as the viscosity of nanofluid.

Except for the case of brick nanofluids Nu's of nanofluids are much larger than Nu of water in the case of ϕ=0.01. This tendency is much more conspicuous with increasing particle loading. Hence, nanofluids appear to be excellent heat transfer fluids. However, we may give a different interpretation for the result. In the present experiment the range of fluid velocity is virtually the same for water and nanofluids, and the range of Nusselt number remains within a similar range. The large change occurs only in Reynolds number. This is due to the large change in zero shear viscosity.

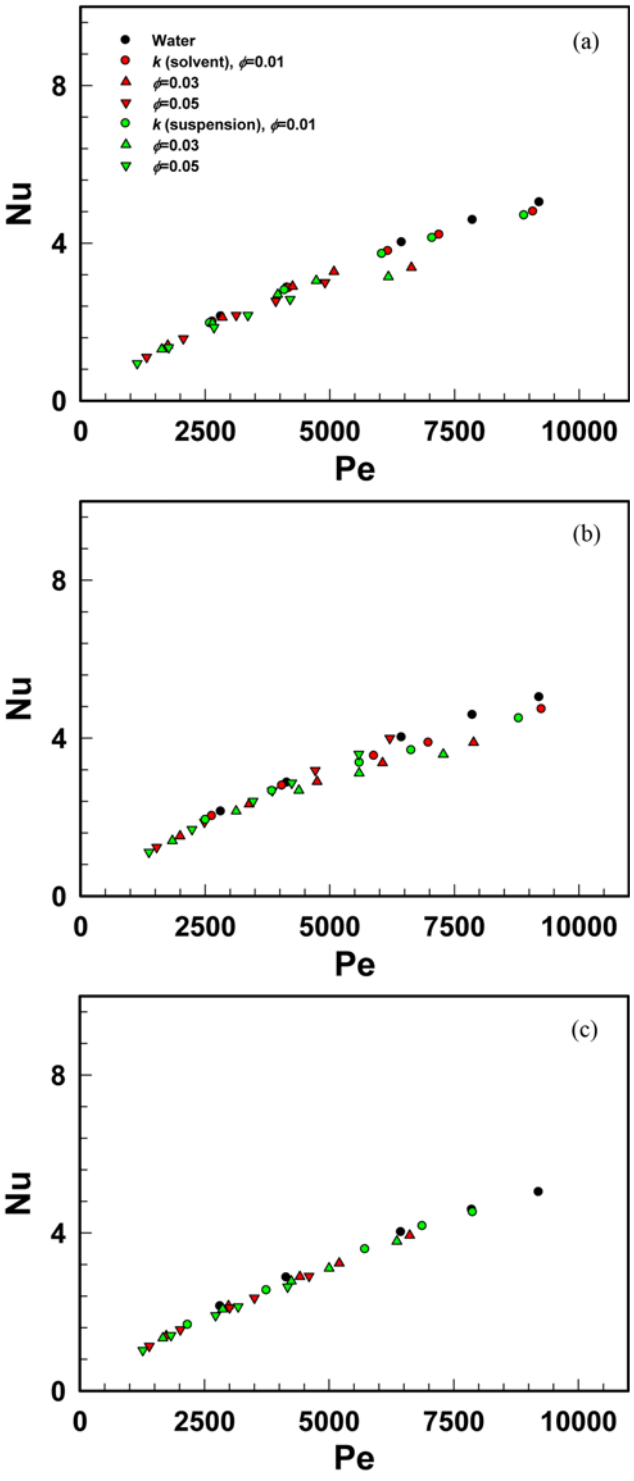

Fig. 7. Nu variation with Pe of nanofluids with different particle shapes. (a) Cylinders, (b) bricks, (c) blades.

Fig. 6 also shows the change in Nusselt number by black symbols with Reynolds number for nanofluids of various nanoparticle shapes and particle loading. Here we used the properties of water in calculating Nu and Re of nanofluids not to exaggerate the heat transfer enhancement. In the figure we have plotted Nu as a function of Re rather than Pe even though Nu is a function of Pe in laminar flows. This is because the friction factor was expressed as a function of Re in the above. By using the same abscissa we can assess the nanofluid more easily. Also, Pe=RePr is proportional to Re and the Prandtl number is the same since we used the property of water, so there should be no confusion. When particle loading is 0.01, Nu of the nanofluid is much the same as that of water. When particle loading is 0.03 or 0.05 there is a tendency that Nu of a nanofluid becomes slightly smaller than that of water at the same Reynolds number. In Fig. 7, Nu of nanofluid is plotted as a function of Pe. Nu of water is virtually the same as Nu of nanofluids especially at low Pe. At Pe>5,000 Nu of nanofluids is even smaller than Nu of water. This implies that the nanofluid may not have advantages as a heat transfer fluid.

We now consider the reason why the difference in heat transfer coefficient between the alumina nanofluid and pure water is small for the present case. As already described, aggregated particles can migrate to the center of the tube in the nonhomogeneous flow field. Then the wall layer contains only a smaller amount of particles, and hence the thermal conductivity becomes smaller than the average value even though some Brownian particles remain in the region. Another reason may be due to the change in the product of density and heat capacity of the nanofluid from the pure fluid. In the laminar tube flow of a homogeneous fluid, the Nusselt number is proportional to Reynolds number from the Leveque approximation [2], thus:

$$h \propto (v\rho C_p)^{1/3} k^{2/3} \tag{11}$$

Here we assume that the same relation can be applied to nanofluids to get insight into the effect of change in ρC_p at least qualitatively. Fig. 8 shows the change in ρC_p with particle loading. The value decreases with particle loading continuously. There is, for example, 1.3% of ρC_p decrease from the water value when particle loading is 0.05. This appears to be a significant loss. Even though

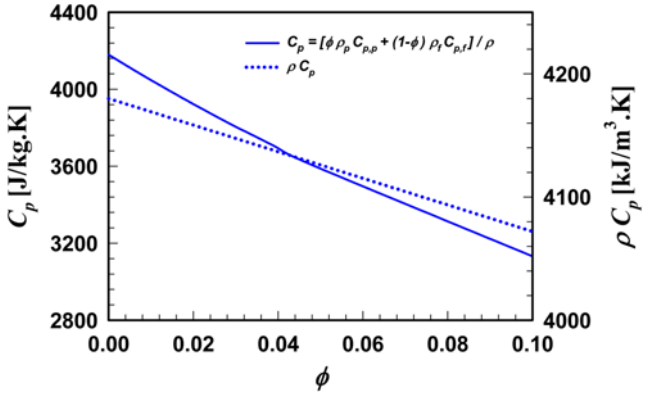

Fig. 8. Density and heat capacity changes of alumina nanofluids with particle loading.

k increases by adding particles, the effect of added particles can be shaded unless k increases substantially. The shear-rate dependent thermal conductivity should influence the convective heat transfer, too. In our previous study, we found that the thermal conductivity of a nanofluid decreased with increasing shear-rate and approached the value of the solvent [29].

CONCLUSION

We investigated the convective heat transfer characteristics of alumina nanofluids containing nanoparticles of different shapes (rods, blades, and bricks) in forced laminar tube flows. The experiments were performed at the thermal entrance regime. We measured the viscosities of nanofluids to characterize them rheologically. First, we validated the heat transfer system by using water and compared the data with the data obtained for nanofluids. It has been found that heat transfer coefficients of nanofluids are almost the same or a little smaller than that of water. The reduction of heat transfer coefficient has been ascribed to the lowering of thermal conductivity of nanofluid under a shear condition and the particle depletion by the cluster migration from the wall to the tube center. Also, the reduction in thermophysical properties appears to contribute to the reduction in heat transfer coefficient.

In many previous studies the Nusselt and Peclet numbers were calculated by using the viscosity and thermal conductivity of nanofluid rather than the properties of the dispersing fluid. We found that this method can cause serious misunderstanding in the interpretation of heat transfer characteristics.

To utilize nanofluids practically, nanofluids should have large thermal conductivities as well as high values of density and heat capacity. Also, they should be well dispersed in liquids without forming large aggregates. Until now we have not been able to find a nanofluid that satisfies all of these requirements. Considering that metal oxide particles form large aggregates or gels in suspensions, nanofluids from metal particles with appropriate stabilizing agents appear to satisfy the requirements.

ACKNOWLEDGEMENTS

This work was supported by the Energy-Resources Technology R&D Program of the Ministry of Knowledge Economy, Republic of Korea (Project No. 2008ECM11P080000). The alumina nanoparticles were donated by Dr. Yun Chang of North American Sasol Inc.

NOMENCLATURE

Br : brinkman number [-]
c_p : heat capacity [$Jkg^{-1}K^{-1}$]
D : diameter of pipe [m]
h : convective heat transfer coefficient [$Wm^{-2}K^{-1}$]
I : electrical current [A]
k : thermal conductivity [$Wm^{-1}K^{-1}$]
L : pipe length [m]
Nu : nusselt number [-]
ΔP : pressure difference [Pa]
Pe : peclet number [-]
Pr : prandtl number [-]
Q : average volumetric flow rate [m^3s^{-1}]
Re : reynolds number
R : radius of pipe [m]
V : electrical voltage [V]
z : position in the axial direction [m]

Greek Letters

μ : viscosity [Pa·s]
ρ : eensity [kgm^{-3}]
ϕ : volumetric particle fraction [-]

Subscripts

avg : average
h : hydraulic
LM : logarithmic mean
NF : nanofluid
p : particle
w : wall

REFERENCES

1. J. A. Eastman, S. R. Phillpot, S. U. S. Choi and P. Keblinski, *Annu. Rev. Mater. Res.*, **34**, 219 (2004).
2. W. M. Deen, *Analysis of transport phenomena*, Oxford University Press, New York, Oxford (1998).
3. H. Chen and Y. Ding, *Advances in Transport Phenomena*, **1**, 135 (2009).
4. V. Y. Rudyak, A. A. Belkin and V. V. Egorov, *Technol. Phys.*, **54**, 1102 (2009).
5. B. Pak and Y. I. Cho, *Exp. Heat Transfer*, **11**, 151 (1998).
6. X. Wang, X. Xu and S. U. S. Choi, *J. Thermophys. Heat Transfer*, **13**, 474 (1999).
7. S. K. Das, N. Putra and W. Roetzel, *Int. J. Heat Mass Transfer*, **46**, 851 (2003).
8. R. Prasher, D. Song and J. Wang, *Appl. Phys. Lett.*, **89**, 133108 (2006).
9. L. Liao and Z. H. Liu, *Heat Mass Transfer*, **45**, 1129 (2009).
10. K. Kwak and C. Kim, *Korea-Australia Rheol. J.*, **17**, 35 (2005).
11. Y. Ding, H. Alias, D. Wen and R. A. Williams, *Int. J. Heat Mass Transfer*, **49**, 240 (2006).
12. H. Chen, Y. Ding and C. Q. Tan, *New J. Phys.*, **9**, 367 (2007).
13. P. K. Namburu, D. P. Kulkarni and D. Misra, *Exp. Therm. Fluid Sci.*, **32**, 397 (2007).
14. Y. Xuan and Q. Li, *ASME J. Heat Transfer*, **125**, 151 (2003).
15. D. Wen and Y. Ding, *Int. J. Heat and Mass Transfer*, **47**, 5181 (2004).
16. R. K. Shah, Proc. of 3rd National Heat Mass Transfer Conference, vol. 1, Indian Institute of Technology, Bombay, p. HMT-11-75 (1975).
17. S. Z. Heris, G. Etemad and M. N. Esfahany, *Int. Comm. Heat Mass Transfer*, **33**, 529 (2006).
18. W. Daungthongsuk and S. Wongwises, *Renewable and Sustainable Energy Reviews*, **11**, 797 (2007).
19. W. Yu, D. M. France, J. L. Routbort and S. U. S. Choi, *Heat Transfer Engineering*, **29**, 432 (2008).
20. S. Kakac and A. Pramuanjaroenkij, *Int. J. Heat Mass Transfer*, **52**, 3187 (2009).
21. V. I. Terekhov, S. V. Kalinina and V. V. Lemanov, *Thermophysics*

Aeromechanics, **17**, 157 (2010).
22. L. Godson, B. Raja, D. M. Lal and S. Wongwises, *Renewable and Sustainable Energy Review*, **14**, 629 (2010).
23. S. M. S. Murshed, C. A. Castro, M. J. V. Lourenco, M. L. M. Lopes and F. J. V. Santos, *Renewable and Sustainable Energy Review*, **15**, 2342 (2011).
24. B. Chun, H. Kang and S. Kim, *Korean J. Chem. Eng.*, **25**, 966 (2008).
25. D. J. Faulkner, D. R. Rector, J. Davidson and R. Shekarriz, *Proceedings of IMECE 2004*, **219** (2004).
26. Y. Yang, Z. George Zhang, E. A. Grulke, W. B. Anderson and G. Wu, *Int. J. Heat and Mass Transfer*, **48**, 1107 (2005).
27. U. Rea, T. McKrell, L. Hu and J. Buongiorno, *Int. J. Heat and Mass Transfer*, **52**, 2042 (2009).
28. S. Ferrouillat, A. Bontemps, J. Ribeiro, J. Gruss and O. Soriano, *Int. J. Heat and Fluid Flow*, **32**, 424 (2011).
29. S. Kim, C. Kim, W. Lee and S. Park, *Rheologica Acta*, (Submitted) (2011).
30. M. P. Escudier, F. Presti and S. Smith, *J. Non-Newtonian Fluid Mech.*, **81**, 197 (1999).
31. W. K. Gingrich, Y. I. Cho and W. Shyy, *Int. J. Heat Mass Transfer*, **35**, 2823 (1992).